Chapter 6
Free-space Optical (FSO) Platforms: Unmanned Aerial Vehicle (UAV) and Mobile

Arun K. Majumdar

6.1 Introduction

This chapter discusses the emerging technology of unmanned aerial vehicle (UAV)-based free-space optical (FSO) communication links. UAVs are a possible future application for both civil and military use. The large amount of data generated by the UAVs requires high data rate connectivity, thus making FSO communication very suitable. This chapter discusses some important issues using FSO links such as the FSO unit alignment and the beam attenuation/fluctuation due to the atmosphere. The technical challenges for the alignment in tracking and acquisition are addressed. Detailed descriptions are provided in the following areas: alignment and tracking of a FSO link to a UAV, short-length Raptor codes for mobile UAV, and a modulating retroreflector (MRR) FSO communication terminal on a UAV. A new methodology of using multiple UAVs in a cooperative swarm mode is also described. Specific areas for UAV swarms are discussed, such as large and adaptive beam divergence for inter-UAV FSO communication, networking architectures, reliability, and appropriate modulation scheme (pulse position modulation, PPM/on-off keying, OOK; incoherent detection). Another section of this chapter deals with the problem associated with mobile platforms, i.e., tracking in moving vehicles and gimbals. The challenges addressed are: variation in receiver beam profile of the FSO link and variation in received optical power due to constantly changing transmitter/receiver separation. Some basic building blocks for high-speed mobile ad hoc networks (MANET) using FSO is described with protocols operating under high mobility. An FSO structure is described which can achieve angular diversity, spatial reuse, and are multielement. The link performance of mobile optical links in the presence of atmospheric turbulence is provided for a FSO-based mobile sensor network. Mobile communication challenges and potential solutions are discussed.

6.2   UAV FSO Communications

Research in the area of FSO communications is usually based on point-to-point link or long-range link for space applications. Mobility, i.e., relative movement of either the transmitting or receiving terminal (or both) is the greatest challenge in the family radio service (FRS) communication technology. By including UAV to provide a communication terminal, a number of flexible and practical applications can be developed. There is increasing interest in UAV for many applications, especially in the area of surveillance, due to zero risk of human casualty. With improved high-resolution imaging sensors that are much higher date rate than radio frequency (RF) technology can support, it is that communication links that transmit more information between UAV and ground terminal, or between UAVs. In order to meet the increasing demand, efficient ways to communicate with UAVs with FSO optics are needed since the UAVs are moving platforms.

Many commercial FSO links operate at 1–2 Gbps over ranges of 1–3 km. Most FSO links are stationary but they have been considered for mobile applications. Some of the applications include ship-to-ship [1], ground-to-air, and air-to-air [2, 3] communication systems and even deep-space communications [4].

6.2.1   UAV Scenarios for FSO Communications Link

There are three basic FSO communications link scenarios with UAV platform. These are (i) ground-to-UAV, (ii) UAV-to-ground, and (iii) UAV-to-UAV or between UAVs (UAV swarm).

Ground-to-UAV Mobile FSO Channel Figure 6.1 shows the ground-to-UAV mobile FSO link where the speed of the UAV can reach several hundred meters per second. Tracking in this scenario is typically accomplished by mechanical components such as a 2-D rotating gimbal which is oriented based on global positing system (GPS) data from the UAV. Small divergent angle of the transmitting beam makes the tracking task difficult. The received signal to noise ratio (SNR) variation can be caused by misalignment of the transmitted beam and the detector due to mechanical pointing uncertainty error and GPS positioning error which limits the data rates of such link [5]. An efficient tracking method is therefore necessary to improve the data rate.

UAV-to- ground FSO Communication Link Figure 6.2 illustrates this concept of a bidirectional daytime and nighttime optical communication link from a UAV to a stationary ground station. One of the tasks the UAV might have is to take science images over desired targets and then download the images via the optical communication channel.

An optical communication terminal receives a command from ground via RF links which also receives continuous updates of the GPS information collected by the UAV GPS receiver. Simultaneously, the UAV provides the optical communication
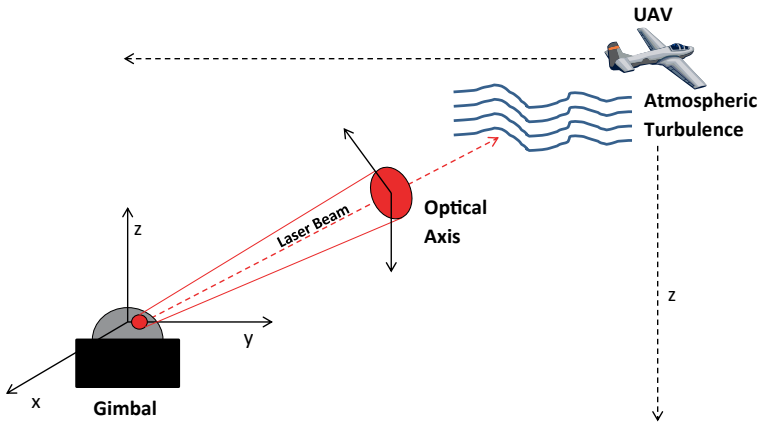
Fig. 6.1 Ground-to-UAV mobile FSO communication. *UAV* unmanned aerial vehicle, *FSO* free-space optical
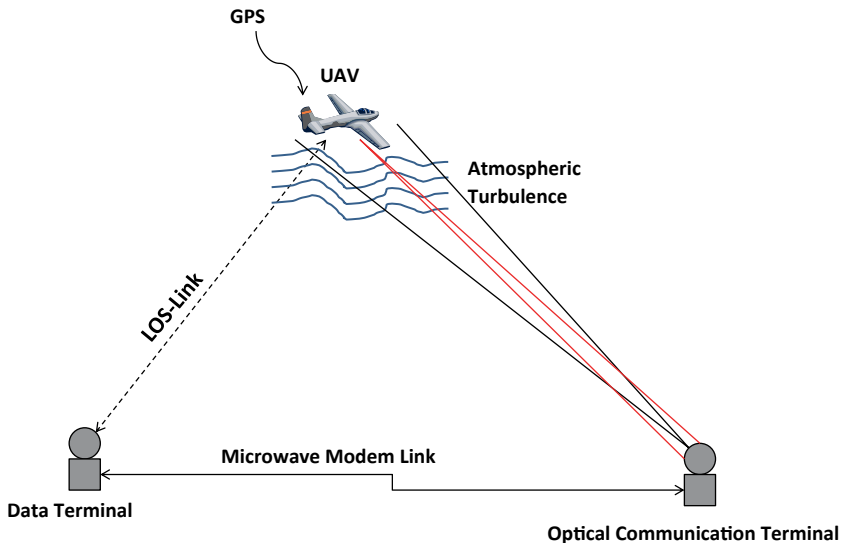

Fig. 6.2 UAV-to-stationary ground station FSO communication. *UAV* unmanned aerial vehicle, *FSO* free-space optical

terminal with its GPS information. The optical communication terminal uses updated information from both the UAV GPS receiver and the ground location to blind point the gumball by sending a beacon signal to initiate the communication signal. Data communication starts when the signal terminal tracks on the beacon signal. A demonstration of the FSO communication link at 2.5 Gbps is presented [6] for a UAV altitude of 15.8–18.3 km using a 200 mW downlink laser at 1,550 nm. They reported bit error rate (BER) of 10^{-9} which needed the pointing requirement on the flight terminal of 19.5 µrad and a bias error of 14.5 µrad with a probability
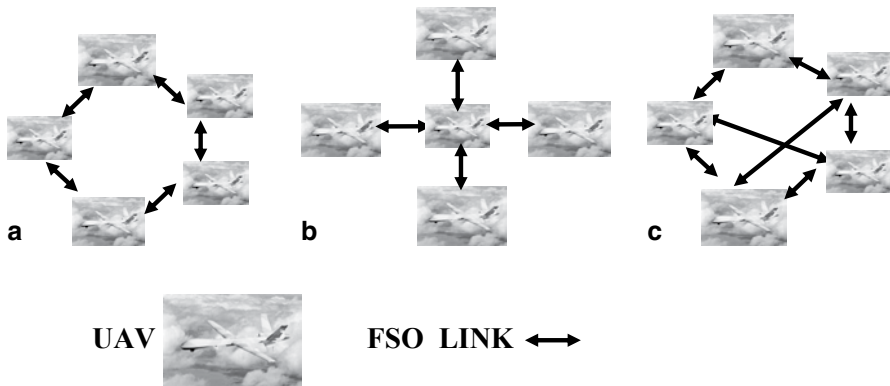
Fig. 6.3 *FSO* network for swarm *UAV*s using three different architecture. **a** Ring Architecture. **b** Star Architecture. **c** Meshed Architecture

of pointing-induced fades (due to turbulence) of 0.1 %. Vibration uncertainties also need to be eliminated for establishing a high data rate communication link.

UAV Swarms; Links Between UAVs The use of UAVs for transferring high date rate information is very rapidly attracting attention. In some situations, it may be necessary to collect data for a defined area with a variety of sensors. When these UAVs are operating in swarm formation, the observation area can be increased and an occasional loss of a UAV will not completely stop the data transfer process using the highly efficient optical communication links. FSO communications offering high bandwidth can therefore provide high data rate connectivity required by the large volume of data in UAV swarms. Figure 6.3 illustrates FSO network for swarm UAVs using three different architectures: *Ring Architecture, Star Architecture, and Meshed Architecture.*

The key point here is to develop the UAVs capabilities to handle multiple sensor information in real-time and in parallel so that a large amount of data can be transferred in real-time with a goal to achieve a rate of 2.5 Gbps or higher.

In the ring architecture mode, all FSO links are bidirectional and in case of a broken (or failure) link between any two UAVs, an indirect link may be used but the information is sent in the other direction where there is still link [7]. In a star architecture, there is one UAV in the middle of the formation which acts as an optical multipoint unit (OMU) [7] and is used as a repeater. All other UAVs equipped with transceivers are permanently connected with this OMU. A failure of the OMU can cause the breakdown of the whole configuration and a redundant OMU might be necessary. A meshed network can provide high reliability by combining the advantages of both the star and the ring architecture. Information flow from one UAV to another can be realized in different forms and can also be sent in the other direction of the ring network.

Atmospheric and Turbulence Effects For different UAV scenarios, the atmosphere plays different roles. Optical signals propagating in the Earth's atmosphere experience degradation due to absorption, scattering, and turbulence. Absorption and

scattering are caused by the interactions of optical waves with atmospheric gases and particulates, such as aerosols and fog, and result mainly in the attenuation of the signal. Turbulence is caused by the random variations of the refractive index at optical wavelength, and when an optical beam propagates through a turbulent medium atmospheric turbulence causes irradiance fluctuations, beam wandering, and loss of spatial coherence of the optical wave. Three possible propagation configurations are related to the UAV FSO communication links: *uplink, downlink, and horizontal.* Uplink configuration is the propagation of a ground-based terminal to another terminal in space in general via a slant path. Downlink is when the communication link is established from the terminal in space to a ground terminal via a slant path. Horizontal link is defined when both of the communication terminals communicate via horizontal path (either on the ground or in space). Obviously, the three links cause different effects on the received signals in a UAV receiver since the atmospheric models for these three links follow different distributions of atmospheric properties.

Atmospheric Models Related to UAV FSO Communication Links Based upon the measurements, empirical and parametric models of turbulence strength parameter, C_n^2 have been derived and several different models are commonly used to represent the effects of atmospheric turbulence, and are described below; h is altitude (meter) [8]:

i) Hufnagel-Valley (HV) model:

$$C_n^2(h) = 0.00594 \left(\frac{v}{27}\right)^2 (10^{-5}h)^{10} \exp\left(-\frac{h}{1000}\right) + 2.7 \times 10^{-16} \exp\left(-\frac{h}{1500}\right) + A \exp\left(-\frac{h}{100}\right) \quad (6.1)$$

where v is the rms wind speed. Typical value of the parameter, $A = 1.7 \times 10^{-14} \text{ m}^{-2/3}$.

ii) ModifiedHufnagel-Valley (MHV) model:

$$C_n^2(h) = 8.16 \times 10^{-54} h^{10} \exp\left(-\frac{h}{1000}\right) + 3.02 \times 10^{-17} \exp\left(-\frac{h}{1500}\right) + 1.90 \times 10^{-15} \exp\left(-\frac{h}{100}\right) \quad (6.2)$$

(iii) Submarine Laser Communication (SLC)-Day model:

$$
\begin{aligned}
C_n^2 &= 0 & 0\,\text{m} < h < 19\,\text{m} & \quad (6.3)\\
&= 4.008 \times 10^{-13} h^{-1.054} & 19\,\text{m} < h < 230\,\text{m} &\\
&= 1.300 \times 10^{-15} & 230\,\text{m} < h < 850\,\text{m} &\\
&= 6.352 \times 10^{-7} h^{-2.966} & 850\,\text{m} < h < 7000\,\text{m} &\\
&= 6.209 \times 10^{-16} h^{-0.6229} & 7000\,\text{m} < h < 20,000\,\text{m} &
\end{aligned}
$$

(iv) CLEAR1 model:

Note: Here h is altitude in kilometer above mean sea level (MSL)

$1.23 < h \le 2.13$

$\log 10\left(C_n^2\right) = A + Bh + Ch^2$

where $A = -10.7025, B = -4.3507, C = +0.8141$

$2.13 < h \le 10.34$ (6.4)

$\log_{10}\left(C_n^2\right) = A + Bh + Ch^2$

where $A = -16.2897, B = +0.0335, C = -0.0134$

$10.34 < h \le 30$

$\log_{10}\left(C_n^2\right) = A + Bh + Ch^2 + D\, exp\{-0.5\left[(h-E)/F\right]^2\}$

where $A = -17.0577, B = -0.0449, C = -0.0005$

$D = 0.6181, \quad E = 15.5617, F = 3.4666$

For an uplink laser communication link, i.e., from a ground-based terminal transmitting to a UAV, the atmospheric turbulence begins just outside the transmitter aperture, and we can assume a spherical wave for propagation. HV model turbulence profile is used. For a specific modulation scheme such as OOK modulation, and knowing the parameters such as wavelength, UAV height, transmitter divergence angle, and a data rate, the UAV communication performance BER can be computed [8]. The BER calculation is based on a Gamma-Gamma probability density function for the intensity fluctuations of the outgoing beam.

For a downlink path from a UAV to a ground terminal, the ground-level scintillation near the center of the received wave can be accurately modeled by a plane wave. The Rytov variance (i.e., intensity variance of a plane wave) in this case depends mostly on high-altitude turbulence, and is consistent with weak-fluctuation theory except the case of very large zenith angle of the UAV. The system performance denoting BER can be calculated using OOK modulation. The same HV model (as was used in uplink model) can be used. Probability of fade variation is similar to the uplink case [8].

For the horizontal case the value of C_n^2 remains constant along the propagation path. The value of C_n^2 at the altitude of the UAVs needs to be accounted for when estimating intensity fluctuations or beam wander.

When the UAVs have to operate under atmospheric scattering conditions, scattering of optical wave by aerosol particulates and fog can be important. The proposed model for short distance link is the Kruse model [7] which relates the attenuation to visibility V (in km) for a given wavelength (in nm). In visible and near infrared (IR) wavelength up to about 2.5 μm, the attenuation is given by [7]:

$$\gamma(\lambda) \approx \beta_a(\lambda) = \frac{\ln(\tau_{TH})}{V}\left(\frac{\lambda}{550nm}\right)^{-q} = \frac{3.912}{V}\left(\frac{\lambda}{550nm}\right)^{-q} \qquad (6.5)$$

where τ_{TH} is the transmission.

The attenuation a_{dB} over the link path distance d_{link} can be calculated from the measured transmission τ or the extinction coefficient $\gamma(\lambda)$ (in km^{-1}) using the following relation:

$$a_{dB} = 10\log\left(\frac{1}{\tau}\right) = \frac{10}{\ln(10)}\gamma(\lambda)d_{link} \qquad (6.6)$$

Results are presented using simulation, [9], for 1 km distance between two UAVs and a divergence angle of 50 mrad giving a system power of 11 mW for clear sky conditions. Results show that 113 mW of transmitter power is needed for moderate fog conditions. For a 2 km distance, the required powers are increased: 44 mW for clear sky and 4.6 W for foggy weather conditions needed.

6.2.2   Alignment and Tracking of a FSO Communications Link to a UAV

For establishing a successful FSO communication link between a ground station and a UAV, the most important criteria to start with is to make sure that the mechanical gimbal can accurately track the moving UAV in presence of atmospheric turbulence. From UAV side, it is important that the minimum transmitting beam divergence is such that the probability of fading of the signal reaching the receiver due to beam wandering caused by atmospheric turbulence is below a required threshold. The repeatability and the accuracy of the gimbal to align and track a ground-to-UAV FSO link needs to be verified. Divergence of the transmitting beam is one technique to help with alignment and tracking of FSO link.

Tracking Algorithm Example for a UAV and a Moving Station (Both Moving Vehicles) Two scenarios are considered to discuss about tracking algorithm: The first scenario is a UAV communicating with a moving vehicle station, and the second scenario is a manned aerial surveillance vehicle with an UAV.

UAV and moving vehicle station: The tracking algorithm sends steering commands to the gimbals so that laser alignment is maintained. The gimbals' angular positions and velocities are specified by the tracking algorithm. The angular position and velocity of the gimbals can be determined by the following equations [10]:

$$\theta = \arctan\left(\frac{z + z_P + z_R + z_Y}{y + y_Y}\right) \qquad (6.7)$$

and

$$\alpha = \arctan\left(\frac{y + y_Y}{x + x_Y}\right) \qquad (6.8)$$

$$\theta' = \frac{(\theta_2 - \theta_1)}{t}$$

$$= \frac{\left(\arctan\left(\dfrac{z_{t1} + z_{Pt1} + z_{Rt1} + z_{Yt1}}{y_{t1} + y_{Yt1}} \right) - \arctan\left(\dfrac{z_{t0} + z_{Pt0} + z_{Rt0} + z_{Yt0}}{y_{t0} + y_{Yt0}} \right) \right)}{t} \quad (6.9)$$

and

$$\alpha' = \frac{(\alpha_2 - \alpha_1)}{t}$$

$$= \frac{\left(\arctan\left(\dfrac{y_{t1} + y_{Yt1}}{x_{t1} + x_{Yt1}} \right) - \arctan\left(\dfrac{y_{t0} + y_{Yt0}}{x_{t0} + x_{Yt0}} \right) \right)}{t} \quad (6.10)$$

where x and y are the distance between the two vehicles on the x-axis and y-axis, respectively at a given time, α is the angular position of the gimbals in the x-y plane, i.e., the yaw, θ is the angular position of the gimbals in the z-y plane, i.e., the pitch, and z is the position of the vehicles on the z-axis. The other variables containing z also denote the z-axis position, but affected by various forces, Z_P is the z-axis position of the vehicle affected by the change in pitch of the vehicle, Z_R by the change in roll of the vehicle, and, Z_Y by the change in yaw of the vehicle. y_Y is the y-axis position of the vehicle affected by the change in yaw of the vehicle. t_0 and t_1 are the times for the vehicles at positions one and two, respectively. x_Y is the x-axis position of the vehicle affected by the yaw of the vehicle. The parameters are determined by the GPS, an inter-vehicular information system (IVIS), and an inertial navigation system (INS). The divergence of the laser source increases proportionately with the increase in distance between the vehicles so that the spread of the light can determine the update rates of the system. As opposed to stationary terminals in the conventions FSO system, when the UAV and another vehicle are moving the mobility causes the most challenge in aligning the two terminals for a successful FSO communication. If we know the various positioning systems as outlined here, an efficient tracking is achievable. This tracking method can be used for transferring real-time video between UAV and a ground vehicle using high bandwidth FSO communications.

Link Margin Analysis for Ground-to-UAV FSO Communications Link Link margin analysis requires calculating the geometric loss for a given transmitter, the transmitter initial beam shape, beam width, and the propagation path length. The transmitter input beam profile $2W_0$ is related to the complex amplitude of the amplitude wave, $U_0(r, 0)$ as follows:

$$U_0(r,0) = A_0 \, \exp\left(-\frac{r^2}{W_0^2} - \frac{ikr^2}{2F_0} \right) \quad (6.10)$$

where α_0 is the amplitude of the wave at the optical axis, F_0 is the radius of curvature of an assumed parabolic distribution of the phase, r is the distance from the beam center line in the transverse direction, and k is the optical wave number. Another parameter is α related to spot size and phase front radius of curvature by the following relation:

$$\alpha = \frac{2}{kW_0{}^2} + i\frac{1}{F_0} \tag{6.11}$$

For link margin analysis based on atmospheric loss only (i.e., no turbulence is considered for this analysis), we need to evaluate geometric loss in FSO communication which is the ratio between the receiving optics and the beam spot size in the receiver plane of the FSO link. Using the Eq. (6.10) for the transmitting lowest-order transverse electromagnetic Gaussian beam wave, with W_0 as the effective beam radius, the beam radius at the receiver plane is given by [11]:

$$W(t) = W_0 \left[\left(1 - \frac{\{[x_u(t)-x_g]^2 + [y_u(t)-y_g]^2 + [h_u(t)-h_g]^2\}^{1/2}}{F_0} \right) \right. \tag{6.12}$$
$$\left. + \left(\frac{2\{[x_u(t)-x_g]^2 + [y_u(t)-y_g]^2 + [h_u(t)-h_g]^2\}}{kW_0} \right) \right]^{1/2}$$

where (x_g, y_g, h_g) are the coordinates of the ground station and $[x_u(t), y_u(t), h_u(t)]$ are time-varying coordinates of the UAV. The Gaussian beam at the receiver plane of the link can be expressed as:

$$U_0(r,L) = A_0(\Theta - i\Lambda)\exp\left(ikL - i\frac{r^2}{W^2}\frac{kr^2}{2F} \right) \tag{6.13}$$

$$\text{where } \Theta = 1 + \frac{L}{F}, \; \Lambda = \frac{2L}{kW^2} \tag{6.14}$$

Their simulated results show that at 1.55 μm wavelength, for a 4-km UAV altitude, an effective beam spot size of 3.03 m, and for a 8-km UAV altitude, an effective spot size of 4.79 m which resulted in expected geometric loss values of −14.8 and −16.8 dB for the 4-km and 8-km altitudes, respectively [12]. Using a receiver threshold sensitivity value of −43 dBm, and factoring in the geometric loss, the pointing loss and optical loss, the FSO receiver threshold sensitivity to only atmospheric loss was found to be −11.3 dBm [11].

6.2.3   FSO Communication Links Using UAV(s): Practical Issues and Recent Development

To establish a UAV FSO link for communication, there are two important factors to be considered: first, to verify that that a UAV FSO link for a ground-to-UAV,

UAV-to-ground, or between UAVs be aligned and then tracked in presence of at-
mospheric turbulence. Both repeatability and accuracy of the gimbal need to be
measured. Also how the beam divergence affects the gimbal's steering tolerance
for expected geometrical losses from the configuration should be evaluated. Some
of the characteristics of the gimbal's ability are investigated [3]. Their experiment
simulated a scenario where a UAV follows a circular flight path of radius 4 km at
an altitude of 4 km for a gimbal elevation of 45° from horizontal and a transmitter-
receiver separation of 5.66 km Their experimental results show the following:

- *X-Y* scatter plot of the gimbal repeatability (fell in an area of 0.5 mm^2) and ac-
  curacy data (gimbal error ranges between 0 and 0.2 mm).
- Distribution of azimuth and elevation repeatability in meters and in degrees:
  azimuth repeatability mean of 1.24 m (226.89 µrad) with a standard deviation of
  0.2 m (52.36 µrad); gimbal elevation repeatability of 0.41 m (69.81 µrad); and
  standard deviation of 0.22 m (39.91 µrad).
- The gimbal pointing error has a mean of 0.3 m (55.85 µrad) with a standard de-
  viation of 0.2 m (34.91 µrad).
- Based on the total variance of intensity versus pointing error, the signal level
  is shown to drop below a threshold of 30 dB to be 3.69×10^{-29} (a very small
  number!).

Their results concluded that the beam divergence present in the FSO link is suffi-
cient to offset any error introduced into the alignment and tracking algorithm by the
gimbal with a very low probability of signal fade for a ground-to-UAV FSO link.

A custom designed and manufactured gimbal with a wide field-of-view (FOV)
and fast response time is presented [12]. This gimbal system is a 24 V system,
with integrated motor controllers and drivers which offers a full 180° FOV in both
azimuth and elevation. Thus, it provides a more continuous tracking capability as
well as increased velocities of up to 479 per second, as well as active and passive
vibration isolation systems. Their design will improve the accuracy and stability
of the precision laser pointing system required for UAV FSO communication link.

Adaptive Beam Divergence Technique:

New technique based on adaptive beam divergence is presented [13] for inter-
UAV FSO under varying distance conditions. A single beam divergence employed
in the link of optical communications may limit the transmission distance between
UAVs. An adaptive beam divergence can improve the free space communication
link performance and provides advantages over a fixed beam divergence in the in-
ter-UAV FSO. The general link equation can be written as:

$$P_{rx} = P_{tx} \cdot L_{rx} \cdot G_{tx} \cdot L_p \cdot L_R \cdot L_{atm} \cdot G_{rx} \cdot L_{rx} \tag{6.15}$$

where P_{rx} is the received power, P_{tx} = transmit power, G_{tx} = transmit optics effi-
ciency, L_P = transmit gain, L_R = pointing loss, L_{atm} = atmospheric loss, G_{rx} = receiver
gain, and L_{rx} = receiver optics loss. If we combine the transmit gain, range loss,
and receiver gain into a single term, geometrical loss, L_{geo}, the Eq. (6.15) can be
re-written as:

$$P_{rx} = P_{tx} \cdot L_{geo} \cdot L_p \cdot L_R \cdot L_{atm} \cdot L_{rx} \qquad (6.16)$$

$$L_{geo} = [a_{rx} / (\theta_{div} \cdot R)]^2 \qquad (6.17)$$

$$L_p = \exp[-8 \cdot (\theta_{err} / \theta_{div})^2] \qquad (6.18)$$

where α_{rx} = receiver aperture diameter, θ_{div} = beam divergence, R = communication range, and θ_{err} = pointing error.

When two UAVs are trying to establish a communication link, knowledge of each other's location is required provided either by a ground control relay or through the swarm control channel. An exact instantaneous position for each UAV is difficult because of its inaccuracy in its on-board positioning system and an uncertainty area is developed in which the measured UAV position and the actual UAV position can be anywhere. The size of the uncertainty area is described by its diameter d_{uca}. Platform jitter, θ_{jitter} can be neglected if it is very small compared to the uncertainty area angular size, i.e.,

$$\theta_{div} \geq \theta_{uca} + \theta_{jitter} \qquad (6.19)$$

An optimum beam divergence is to be determined now in order to deliver more beam power to the edge of the uncertainty area so that UAV at that location will receive sufficient beam power to continue communications. From Eqs. (6.17) and (6.18), a larger beam divergence will increase the geometrical loss and the pointing loss will be reduced for a fixed pointing error. From the Eqs. (6.17) and (6.18), we can find the optimum beam divergence to send the most beam power to the edge of the uncertainty area while satisfying the condition, Eq. (6.19). The distance between the two communicating UAVs is continuously changing which affects the maximum angular pointing error, which is the maximum mispointing of beam when the UAV is the edge of the uncertainty area defined by [13]:

$$\theta_{max-err} = 0.5 \cdot (d_{uca} / R + \theta_{jitter}) \qquad (6.20)$$

Instead of increasing the receiver aperture size or transmit power, a more efficient method is to adopt an adaptive beam divergence to mitigate the loss due to the distance under the constraint of Eq. (6.19). Thus, the loss due to the geometrical and pointing loss can be reduced by constantly changing the beam divergence according to the distance. The amount of loss at the edge of the uncertainty area is given by [13]:

$$EdgeLoss = 0.36 \cdot \{a_{rx} / [1.4 \cdot (d_{uca} + \theta_{jitter} \cdot R)]\}^2 \qquad (6.21)$$

For a Gaussian beam, collimated beam diameter is given by [14]:

$$\theta_{div} = (4 \cdot \lambda) / (\pi \cdot d_{out}) \qquad (6.22)$$

where λ is the transmitter wavelength, and d_{out} is the collimated output beam diameter. The collimated beam output can therefore be altered to provide adaptive beam divergence adjustment in order to improve the FSO communication performance under varying distance conditions.

Short-length Raptor Codes for Ground-UAV Optical Channels Recently short-length Raptor codes, independent of channel misalignment caused by tracking error and atmospheric scintillation are presented for a ground-to-UAV mobile FSO channel [5]. A UAV FSO channel can suffer severe instantaneous misalignment which is not known to the transmitter causing data packet corruption and erasure. Traditional fixed-rate erasure coding technique is not suitable. Applications of rateless Raptor codes for such mobile FSO system is presented where short-length (16–1024) Raptor codes are designed to apply to a severe jitter FSO channel. For a 1 Gbps transmitter, the designed Raptor code with $k = 64$ message packets can deliver 560 Mbps data rate for a decoding cost of 4.11 operations per packet with transmitting power of 20 dB. A traditional automatic repeat-request (ARQ) algorithm technique for the same jitter channel can deliver only 60 Mbps. Thus the short-length Raptor code is useful for a ground-to-UAV FSO link performance improvement.

Modulating Retroreflector (MRR)-based UAV FSO Communications Original research on multiple quantum well (MQW) modulating retroreflector started more than 10 years ago at Naval Research Laboratory (NRL) [15]. Modulating retroreflector systems couple an optical corner cube retroreflector and an electro-optic shutter to provide a 2-way optical communications using a laser source and a pointer-tracker on only one platform. The MRR at that time at NRL used a semiconductor-based MQW shutter capable of modulation rates greater than 10 Mbps. Many years ago, they demonstrated an IR data link between a small rotary-wing UAV and a ground-based interrogator using the MQW device designed and fabricated at NRL. Optical link to an UAV in flight at that demonstration covered a range of only 100–200 ft. An airborne reconnaissance concept using a UAV was presented with MQW MRR [15]. When using an array, the MQW MRR concept reduced the payload requirements for the onboard communication system. The laser communication to small UAVs can have the loose pointing requirements of MRR. Small, lightweight, and low-cost gimbals can therefore be used for pointing. For small UAV, low precision hardware can be used which also decreases size, weight, power, and cost. The MRR transmitter can be much smaller, lighter, and uses less power than a traditional laser transmitter. NRL demonstrated an initial flight test using a small UAV. For a small UAV system, MRR transmitters and photodetectors (PDs) are installed in low-cost, lightweight gimbals. Two wingpods, each contains an MRR gimbal, a photoreceiver gimbal, a stabilized camera, and electronics. Flight tests are reported where live video is transmitted to the ground using the lasercom downlink, whereas pointing and zoom comments are sent to the camera via the lasercom link. A frame captured from a 15 frame/s video stream is shown [16].

A micro-electro-mechanical systems (MEMS)-based modulating retroreflector is proposed as a communication terminal onboard a UAV allowing both the laser

transmitter and acquisition, tracking, and pointing (ATP) subsystems to be elimi-
nated. The ATP in the ground station is based on a GPS-aided two-axis gimbal for
tracking and course pointing, and a fast steering mirror for fine pointing. The system
designed is a beacon-based, taking advantage of the retroreflector optical principle
to determine the UAV position in real-time. A modulating retroreflector has been
proposed as the communications remote terminal where the retroreflector sends the
incoming beam back to the ground station via the same path of the interrogator laser
on the ground. Both liquid-crystal-based and MEMS-based MRR are considered.
With MEMS device, a data rate of >1 Mbps is the goal while keeping the power
consumption to remain below 100 mW with the starting laser beam-width of 0.2 cm
and initial range of 10–1,000 m [17]. An air-to-ground FSO communication system
design is presented with an emphasis to achieve the minimum payload power, size,
and weight using a MEMS modulating retroreflector [18]. A new technique for fine
pointing based on a liquid-crystal device is chosen at the ground station.

Swarm UAVs FSO Communication One of the future applications for UAV fly-
ing in swarm carrying a variety of sensors is for monitoring and surveillance a
large area. Data rates of 100 Mbps to 1 Gbps are needed to handle multiple sensor
information in real time and parallel. For swarm UAVs, a reliable and high-perfor-
mance wireless communication link among UAVs are essential. There are two com-
munication systems needed for the swarm UAVs: Air-to-air UAV communication
system enables the sharing of sensor and map information among the UAVs, and
air-to-ground system provides mission information to the ground station for mission
control and display. Actions of each UAV can reduce the risk in the environment
for all other UAVs. Different types of networks for swarm UAVs were mentioned
earlier in this chapter: Ring, Star, and Meshed Architectures. Links between UAVs
are considered [7] for short links because of high costs. The effects of turbulence
on the propagation path is negligible compared to foggy environments. For short
links, an omnidirectional beam arrangement and the beam broadening are inter-
esting alternate solution to expensive and heavy tracking system. Omnidirectional
multi-beam systems installed on swarm UAVs offer potential enhanced reliability
and availability. Due to continuous motion and changing relative speeds of all its
members, for the swarm UAV scenario to maintain a line-of-sight (LOS) FSO link
is challenging [19].

6.3   Mobile FSO Communications

Originally, the FSO communication was meant for stationary terminals for provid-
ing high bandwidth solution. Introducing mobility to FSO technology will open
more applications. Mobility will also have its own challenges including the LOS
maintenance for continuous data flow. One of the goals is therefore to develop tech-
nology that enables a mobile terminal to be tracked.

Fig. 6.4 *FSO* link configuration for a transmitter and a receiver mounted on mobile platforms. *FSO* free space optical
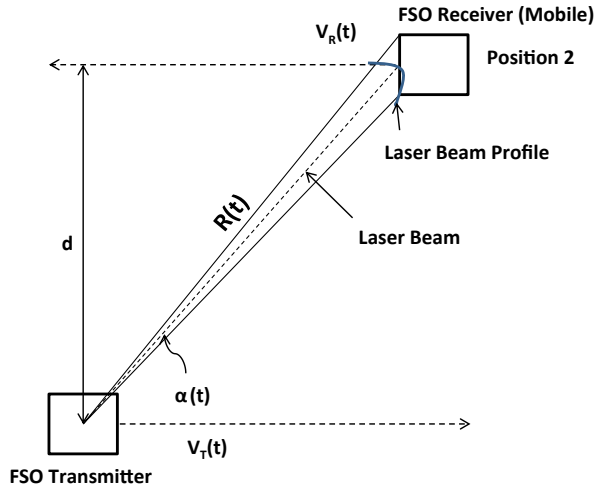
6.3.1 Beam Divergence and Power Levels Variations in Mobile FSO Communications

As the transmitter-receiver separation continuously changes in a mobile FSO link, the received beam profile and the received power levels also change. Beam divergence is used to simplify alignment of transmitter and receiver in FSO link. For a mobile operation using FSO link, the propagation range is continuously changing with time, and therefore the received beam profile on the receiver plane is changing. Consequently the beam divergence is changing with the propagation distance and the received power is also varying. From a communications point of view, the variations in received power cause the SNR to change constantly which results in changes in BER of the systems performance. This simply means that in mobile FSO link, it is difficult to maintain a constant high data rate that is required by the system. The system requires that the received power level should be within the maximum and minimum allowable power levels even if the distance between the transmitter and the receiver terminals changes.

Mobile FSO Link Analysis Figure 6.4 shows a FSO link configuration for a transmitter and a receiver mounted on mobile platforms. The transmitter *Tx* is travelling up with a velocity $v_{Tx(t)}$ and the receiver *Rx* is traveling down with a velocity $v_{Rx}(t)$, the range $R(t)$ between the transmitter and the receiver is varying with time while keeping the horizontal separation d constant while both terminals move. The resulting beam profile on at the receiver plane is $W(t)$. At any time t, the separation between *Tx* and *Rx* is given by:

$$R(t) = \frac{d}{\sin \alpha(t)} \tag{6.23}$$

where $\alpha(t)$ the angle between Tx and Rx is also varying with time. If we assume the lowest order transverse Gaussian beam, $U_0(\bar{r},0)$ for the transmitting beam, then we can write [20]:

$$U_0(\bar{r},0) = A_0 e^{\left(-\frac{r^2}{W_0^2} - j\frac{kr^2}{2F_0}\right)} \tag{6.24}$$

where A_0 is the amplitude of the wave, r is the distance from the center line in the transverse direction, $j^2 = -1$, W_0 is the effective beam radius at the transmitter, F_0 is the parabolic radius of curvature of the phase distribution, and k is the optical wave number. If we substitute α_0 as follows:

$$\alpha_0 = \frac{2}{kW_0^2} + j\frac{1}{F_0} \tag{6.25}$$

then Eq. (6.24) can be written as:

$$U_0(\bar{r},R(t)) = A_0 e^{\left(-\frac{1}{2}\alpha_0 kr^2\right)} \tag{6.26}$$

The optical field at the distance $R(t)$ can be written as Huygens-Fresnel integral [20]:

$$U_0(\bar{r},R(t)) = -2\,\mathrm{jk} \int\!\!\int_{-\infty}^{\infty} G(\bar{s},\bar{r};\ R(t)) U_0(\bar{s},0)\, d^2 s \tag{6.27}$$

where $U_0(\bar{s},0)$ is the optical wave at the source plane, i.e., at the ground station transmitter plane and $(\bar{s},\bar{r};\ R(t))$ is a Green's function. In general, Green's function is a spherical wave which, under the paraxial approximation, can be expressed as [20, 21]:

$$G(\bar{s},\bar{r};\ R(t)) = \frac{1}{4\pi R(t)} e^{\left[jkR + \frac{jk}{2R(t)}|\bar{s}-\bar{r}|^2\right]} \tag{6.28}$$

Evaluating the integrals, a Gaussian-beam wave with complex amplitude $\dfrac{A_0}{1+j\alpha_0 R(t)}$ can be obtained as

$$U_0(\bar{r},R(t)) = \frac{A_0}{1+j\alpha_0 R(t)} e^{\left[jkR(t) - \frac{1}{2}\left(\frac{\alpha_0 kr^2}{1+j\alpha_0 R(t)}\right)\right]} \tag{6.29}$$

where $[1+j\alpha_0 R(t)]$ is the propagation parameter [21]. In terms of the input plane beam parameters, such as beam radius, the following parameters are defined:

$$\Theta_0 = \mathrm{Re}(1+j\alpha_0 R) = 1 - \frac{R(t)}{F_0} \tag{6.30}$$

$$\Lambda_0 = \mathrm{Im}(1 + j\alpha_0 R) = \frac{2R(t)}{kW_0^2} \tag{6.31}$$

The parameter Θ_0 describes the amplitude change in the wave due to focusing, and Λ_0 describes the amplitude change due to diffraction. The receiver parameters can be expressed in terms of the source parameters:

$$\text{and} \quad \Theta = \frac{\Theta_0}{\Theta_0^{\,2} + \Lambda_0^{\,2}} \quad \text{and} \quad \Lambda = \frac{\Lambda_0}{\Theta_0^{\,2} + \Lambda_0^{\,2}} \tag{6.32}$$

where Θ and Λ are the receiver beam parameters. The beam radius W and the phase front curvature F at the receiver are given by [21]:

$$\Theta = 1 + \frac{R(t)}{F}, \ \Lambda = \frac{2R(t)}{kW^2(t)} \tag{6.33}$$

The beam radius at the receiver Rx can be written as:

$$W(t) = W_0(\Theta_0^{\,2} + \Lambda_0^{\,2})^{1/2} = \frac{W_0}{(\Theta^2 + \Lambda^2)} \tag{6.34}$$

The distance between TX and Rx $R(t)$ is related to the angle $\alpha(t)$ between them as shown in the Eq. (6.23). Thus, the beam radius can be written as:

$$W(t) = W_0 \left[\left(1 - \frac{\dfrac{d}{\sin\alpha(t)}}{F_0} \right) + \left(2\frac{\dfrac{d}{\sin\alpha(t)}}{kW_0} \right) \right]^{1/2} \tag{6.35}$$

The Gaussian-beam wave at the receiver is:

$$U_0(\bar{r}, R) = A_0(\Theta - \Lambda)e^{\left(jkR - \frac{r^2}{W^2(t)} - j\frac{krt^2}{2F} \right)} \tag{6.36}$$

The irradiance or intensity of the optical wave is the squared magnitude of the field. Thus at the receiver, the irradiance is given by [20]

$$I^0(r, R) = |U_0(r, R)|^2 \tag{6.37}$$

The total power at the receiver can be calculated from [20]

$$P = \iint_{-\infty}^{\infty} I^0(r, R)d^2r \tag{6.38}$$

Therefore, for mobile terminals (*Tx* and *Rx*), the divergence of the beam and the power can be computed so that the gimbals be rotated by proper aligning in order to improve the performance of the mobile FSO communication link.

Simulation results are presented [22] for a mobile FSO link using the following parameters: a 20 mW laser transmitter operating at a wavelength of 1.55 μm for a constant distance, *d* of 1,000 m, varying angle $\alpha(t)$ from +15° to −15°, and the effective beam radius of the transmitter of 2 cm with a half angle divergence of 100 μrad. The simulation results reported are: The Gaussian beam profile at minimum and maximum transmitter-receiver separation is spread upto 0.67 and 0.18 radial distance, the receiver beam radius for alignment varies from 24.1 to 88.0 cm (this variation on receiver beam profile requires the implantation of a tracking algorithm to take account of this variations), and the received power varies from a maximum of 19.9 mW to a minimum of 16.9 mW for the 20 mW laser transmitter at 1.55 μm.

A tracking control method for an active FSO communication system is presented in [23] that enables a mobile terminal to be tracked in a user network area with short-range coverage. The active FSO system consists of paired terminals of a transmitter with a laser diode (LD) and a receiver with a PD. Each terminal controls the path of the laser beam to align it with the optical axis of the PD regardless of the positional changes between the terminals. An extended Kalman filter method proposed in their work in order to estimate the relative position and orientation between the terminals which is required by the axis alignment control.

For a successful PAT for a FSO links between ground and aerial vehicles is presented [24] with the capability of a high precision, agile, digitally controlled two-degree-of-freedom electromechanical system for positioning of optical instruments, cameras, telescopes, and communication laser.

6.3.2   MANET FSO Communication Links

The recent proliferation of wireless technologies for various user applications have prompted a tremendous wireless demand. Wireless nodes are essential to provide the full ranges of connectivity for gathering and exchanging information anytime, anywhere and are expected to dominate the Internet soon. Smartphones via WiFi and mobile Web allow users to get information anywhere and anytime. There is thus the exploding mobile wireless traffic demand which can only be met by leveraging the enabled optical wireless spectrum with high bandwidth capacity. Ultra-high-speed MANETs with cooperative multiple-input-multiple-output (MIMO) can satisfy today's tremendous wireless demand. This subsection will discuss the basics of FSO MANETs with conceptual node designs.

Mobile FSO Communications and MANETS FSO and MANETs are two areas in telecommunications research that have been shown rapid development over the last several years. A MANET enhanced with FSO communication units would provide improved solutions for telecommunication services where infrastructure is unavail-
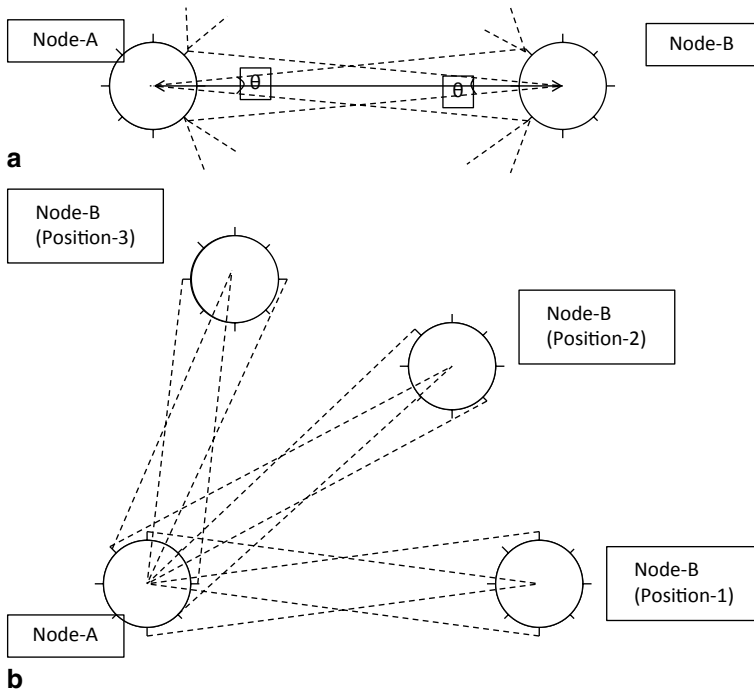
Fig. 6.5 a Multielement optical antenna with an interface having an alignment table on Node A to determine which interfaces of Node B can be aligned. **b** Conceptual scenario for alignment of two nodes (*Reprinted with permission [25])*

able, such as emergency response, disaster recovery, environmental monitoring, etc. The key limitation of FSO for mobile communication is that the LOS alignment has to be maintained all the time during successful communication. The transmitter and receiver pair should be aligned with respect to the focused optical beam with the capability to compensate for any sway or mobility.

For MANET to operate successfully, accurate alignment is essential. A timer-based alignment implementation is presented [25] in auto-alignment circuitry where interface alignment procedure is implemented periodically instead of sending a packet every. A timer is introduced which goes off with a predetermined (roughly 0.5 s) frequency and calculates the alignments in the network. Every transceiver determines its neighbor and keeps a table that has an entry for each aligned transceiver. A basic multielement antenna is shown in Fig. 6.5 (a) where an interface on Node A has an alignment table to determine which interfaces of Node B are to be aligned (those who are within the FOV of Node A). Every transceiver in the network keeps a table for keeping track of its neighboring transceivers which is used for alignment. Only when the interfaces are aligned, the channel delivers the packet to the transceiver. Figure 6.5 (b) shows a mobile scenario with two nodes: Node A (stationary) and Node B (moving). The two nodes lose their alignment when Node B is in an intermediate state, i.e., between position 1 and 2, or between position 2 and 3. In order to maintain the connection between the two nodes, choosing the
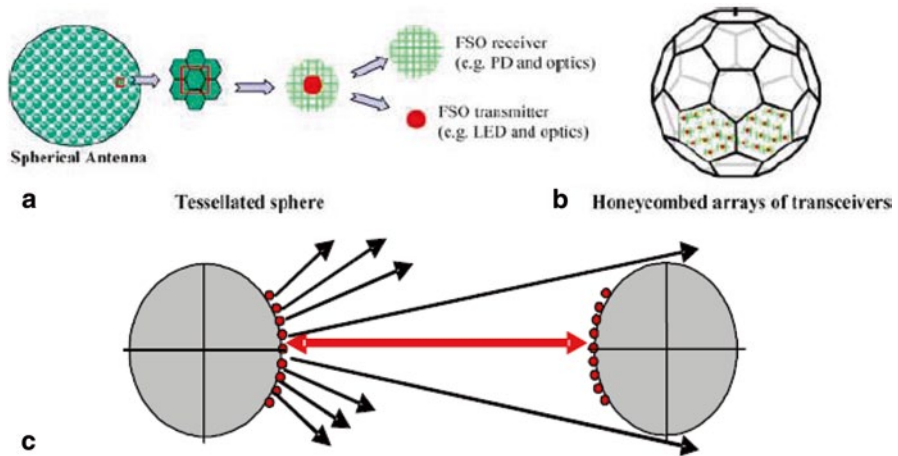
Fig. 6.6 3-D spherical FSO systems with optical transceivers. **a** Translated sphere. **b** Honeycombed arrays of transceivers. **c** 3-D spherical FSO mode showing a line-of-sight (LOS) maintenance(*Reprinted with kind permission from Springer Science+Business Media B.V., 2007, Figs. 1(a), 1(b), and (3)* [26]). *FSO* free-space optical

divergence angle and increasing the number of transceivers may be helpful. An auto-alignment circuitry has been designed [26] to remedy the problem of hand-off. When the two nodes are mobile, the alignment between them is lost and is to be regained, and the two transceivers should be changed in both nodes to accommodate these changes. Auto-alignment circuitry delivers quick response and auto hand-off of logical flows among different transceivers. In the Fig. 6.5 (b), an auto-alignment circuitry in Node A, e.g., will switch from one interface to another interface and finally to an interface in Node B position 1 as Node B changes its position from position 1 to position 2 and position 3, thus handing off the logical stream to a different physical channel. Thus to ensure uninterrupted data flow, auto-aligning transmitter and receiver modules are necessary.

Practical Issues for MANET Alignment and Recent Development MANET design with multi-transceiver optical wireless spherical structures: A concept of spherical FSO node is presented [26, 27]. The spherical FSO node provides the needed angular diversity and LOS in all directions. Figure 6.6 (a) shows the general concept of spherical surfaces where 3-D arrays of FSO transceivers are installed. Each transceiver on the sphere has a transmitter (e.g., Light Emitting Diode, LED) and optical receiver e.g. PD). To minimize the geometric loss due to beam divergence, the transmitter size should be as small as possible, and the receiver as large as possible within one slot of the 3-D array. This arrangement not only improves the range characteristics (availability of light source in every direction) but also enables multichannel simultaneous communication through multiple transceivers. One of the optimum designs includes constructing the nodes in honeycombed arrays of transceivers as shown in Fig. 6.6 (b). An auto-alignment circuitry is also incorporated which selects which transceiver to use for data communication. Figure 6.6 (c) depicts the 3-D spherical FSO node showing a LOS maintenance.

Communication Coverage Propagation Model and Optimal Coverage Higher packaging density can improve communication performance by providing higher aggregate coverage, but also introduces interference of the neighboring transceivers. The coverage area may be defined [27] as the area, points of which are within the LOS of the FSO node. Let r equal the radius of the circular 2-D FSO node (for the purpose of analysis, a 2-D FSO is considered and then a 3-D FSO is analyzed), ρ = the radius of a transceiver, θ = the divergence angle of a transceiver, and τ = the length of the arc in between two neighboring transceivers on the 2-D circular FSO node. For n transceivers placed at equal distance gaps on the circular FSO node, and the diameter of a transceiver 2ρ, τ is then given by [27]:

$$\tau = \frac{2\pi r - n2\rho}{n} = 2\left(\frac{\pi r}{n} - \rho\right) \tag{6.39}$$

The angular difference φ between two neighboring transceivers is given by [27]:

$$\varphi = 360° \frac{\tau}{2\pi r} \tag{6.40}$$

The FSO transceiver's convergence (the vertical projection of a lobe) is approximated as the combination of a triangle and a half circle [27]. Let R be the height of the triangle so that the radius of the half circle is $R \tan\theta$. The coverage area of a single transceiver L can be derived from:

$$L = R^2 \tan\theta + \frac{1}{2}\pi(R \tan\theta)^2 \tag{6.41}$$

The coverage area C of a single transceiver can be found for two cases, (i) coverage areas of the neighbor transceivers do not overlap, and (ii) coverage areas of the neighbor transceivers overlap. The coverage areas of the neighbor transceivers do not overlap when $\tan\theta \leq (R + r)\tan\left(\frac{\varphi}{2}\right)$, and the coverage area is the same as the coverage area, i.e., $C = L$. When the coverage area of the neighbor transceivers overlap, i.e., $\tan\theta \geq (R + r)\tan\left(\frac{\varphi}{2}\right)$, the coverage area is the coverage area excluding the area that interferes with the neighbor transceiver, i.e., $C = L - I$, where I is the interference area that overlaps with the neighbor transceiver's coverage. A prescription and geometry is given in [26] to find the interference area.

The Maximum Range R_{max} The maximum range R_{max} that can be reached by the 2-D FSO node depends on the transmitter's and receiver's optical and electro-optical characteristics, geometry, the atmospheric attenuation, and geometrical spread of the FSO node. The geometric attenuation A_G is a function of the transmitter radius, γ, the radius of the receiver (on the other receiving FSO node) ζ cm, divergence angle of the transmitter θ, and the distance between the transmitting node and receiving node R and is given by [26]:

$$A_G = 10\log\left(\frac{\zeta}{\gamma + 200\ R\theta}\right)^2 \tag{6.42}$$

The atmospheric attenuation A_L depends on the absorption and scattering of the optical transmitting wave by the atmospheric molecules and aerosols and is given by:

$$A_L = 10\log(e^{-\sigma R}) \tag{6.43}$$

where σ is the attenuation coefficient due to both absorption and scattering coefficients. For FSO communications, Mie scattering dominates the other losses and σ (Km) can be written as (in terms of the visibility), V (Km) for a transmitting wavelength λ [28]:

$$\sigma = \frac{3.91}{V}(\lambda/550)^{-q} \tag{6.44}$$

where q is the size distribution of the scattering particles and depends on the visibility V: $q = 1.6$ (for $V \geq 50$ Km, 1.3 (for 6 km $50 \leq V < 50$ Km), and 0.585 $V^{1/3}$ (for V < 6 km).

For a transmitter source power of P dBm and receiver sensitivity $S = -43$ dBm, the following inequality needs to be satisfied for detecting optical signal:

$$S - P < A_L + A_G - (P + 43) < A_L + A_G \tag{6.45}$$

From the inequality, the maximum solution of which is R_{max}:

$$-(P+43) < 10\ log(e^{-\sigma R}) + 10\ log\left(\frac{\zeta}{\gamma + 200R\ \theta}\right)^2 \tag{6.46}$$

R can be solved from the above equation to determine the maximum range for a given FSO transmitter and receiver parameters and atmospheric condition. The optimal number of transceivers that should be placed on the 2-D circular FSO node is obtained by optimizing the total effective coverage area of n transceivers, i.e., nC. Note that C depends on P, θ, V, and n. For a given r and ρ, the optimization problem can be written as [27]:

$$\max_{\theta,\text{P},\text{V},\text{n}}\left\{nC(\theta,P,V,n)\right\} \tag{6.47}$$

As an example, a task can be to optimize the parameters such that 0.1 mRad $\leq \theta$, P $\leq$ 32 mW, and $V \leq$ 20, 200 m.

Development of MANET technology is extremely important for satisfying the high demands for telecommunication for today and for the future.

References

1. V. Gadwal, S. Hammel, Free-space optical communication links in a marine environment. Proc. SPIE. **6304**, 1–11 (2006)
2. T. I. Kin, H. Refai, J.J. Sluss Jr., Y. Lee, Control system analysis for ground/air-to-air laser communications using simulation. Proc. IEEE 24th Digital Avionics Syst. Conf. 1.C.3-1–1.C.3-7 (2005)
3. A. Harris, J.J. Suss Jr., H.H. Refai, Alignment and tracking of a free-space optical communication link to a UAV. Proc. IEEE 24th Digital Avionics Syst. Conf., IEEE Conf. 0-7803-9307-4/05/, 1.C.2-1–1.C.2-9 (2005)
4. A. Biswas, S. Pazzola, Deep-space optical communications downlink budget from mars: System parameters. Interplanetary Network Progress Report, Jet Propulsion Laboratory (2003)
5. W. Zhang, S. Hranilovic, Short-length raptor codes for mobile free-space optical channels. 978-1-4244-3435-009/IEEE ICC Proc. (2009)
6. G.G. Ortiz, S. Lee, S. Monacos, M. Wright, A. Biswas, Design and development of a robust ATP subsystem for the Altair UAV-to-Ground Laesrcom 2.5 Gbps Demonstration. SPIE Proc. **4975**, 103–114 (2003)
7. Ch. Chlestil, E. Leitgeb, S.S. Muhammad, A. Friedl, K. Zettl, N.P. Schmitt, W. Rehm, N. Perlot, Optical wireless on swarm UAVs for high bit rate applications. Proc. IEEE Conf. CSNDSP 19th–21st July, Patras, Greece (2006)
8. A.K. Majumdar, F.D. Eaton, M.L. Jensen, D.T. Kyrazis, B. Schumm, M.P. Dierking, M.A. Shoemake, D. Dexheimer, J.C. Ricklin, Atmoepheric turbulence measurements over desert site using ground-based instruments, kite/tetherd-blimp platform and aircraft relevant to optical communications and imaging systems: Preliminary results. Proc. SPIE **6304**, 63040X-1–63040X-12 (2006)
9. E. Leitgeb, Ch. Chlestil, A. Friedl, K. Zettl, S.S. Muhammad, Feasibility study: UAVs. TU-Graz/EADS, Study (2005)
10. M. Al-Akkoumi, R. Huck, J. Sluss Free-space optics technology improves situational awareness on the battlefield. SPIE Newsroom, 1–3 (2007). 10.1117/2, 1200709.0858
11. A. Harris, J.J. Sluss, H.H. Refai, Free-space optical wavelength diversity scheme for fog mitigation in a ground-to-unmanned-aerial-vehicle communications link. Opt. Eng. **45**(8), 86001 (2006)
12. M. Locke, M. Czarnomski, A. Qadir, B. Setness, N. Baer, J. Meyer, W.H. Semke, High-performance two-axis gimbal system for free space laser communications onboard unmanned aircraft systems. Proc. SPIE. **7923**, 79230M-1–79230M-8 (2011)
13. K.H. Heng, N. Liu, Y. He, W.D. Zhong, T.H. Cheng, Adaptive beam divergence for inter-UAV free space optical communications. IEEE Conf. IPGC (2008)
14. S.G. Lambert, W.L. Casey, *Laser Communications in Space* (Artech House, Boston, 1995)
15. G.C. Gilbreath et al., Large-aperture multiple quantum well modulating retroreflector for free-space optical data transfer on unmanned aerial vehicles. Opt. Eng. **40**(7), 1348–1356 (2001)
16. P.G. Goetz et al., Modulating retro-reflector lasercom systems at the naval research laboratory. The IEEE Military Communications Conference- Unclassified Program- Systems Perspective Track, 1601–1606 (2010). 978-1-4244-8180-410
17. A. Carrasco-Casado, R. Vergaz, J.M. Sanchez-Pena, Design and early development of a UAV terminal and a ground station for laser communications. Proc. SPIE. **8184**, 81840E-1–81840E-9 (2011)
18. A. Carrasco-Casado, R. Vergaz, J.M. Sanchez-Pena, E. Oton, M.A. Geday, J.M. Oton, Low-impact air-to-ground free space communication system design and first results. IEEE Conference on Space Optical Systems and Applications, (2011). 978-1-4244-9685-311

19. S.S. Muhammad, T. Plank, E. Leitgeb, A. Friedl, K. Zettl, T. Javornik, N. Schmitt. Challenges in establishing free space optical communications between flying vehicle. IEEE Proceedings, CSNDSP08, 82–86, (2008). 978-1-4244-1876-308

20. L.C. Andres, R.L. Phillips, *Laser Beam Propagation through Random Media* (SPIE, Bellingham, 1998)

21. A. Ishimaru, *Wave Propagation and Scattering in Random Media* (IEEE, Piscataway, 1997)

22. A. Harris, T. Giuma, Divergence and power variations in mobile free-space optical communications. IEEE Third International Conference on Systems, 174–178 (2008). 978-0-7695-3105-208

23. K. Yoshida, T. Tsujimura, Tracking control of the mobile terminal in an active free-space optical communication system. SICE-ICASE International Joint Conference, 89-950038-5-5 98560/06, Bexco, Busan, Korea, 369–374, (Oct. 18–21, 2006)

24. V.V. Nikulin, J.E. Malowicki, R.M. Khandekar, V.A. Skomin, D.J. Legare, Experimental demonstration of a retro-reflective laser communication link on a mobile platform. Proc. SPIE. **7587**, 75870F-1–75870F-9 (2010)

25. M. Bilgi, Capacity scaling in free-space-optical mobile ad-hoc networks. A Master's Thesis, at the University of Nevada, Reno, May 2008

26. M. Yuksel, J. Akella, S. Kalyanaraman, P. Dutta, Free-space mobile ad hoc networks: Auto-configurable building blocks. Wirel. Netw. (Springer, 2007). doi:10.1007/s11276-007-0040-y

27. M. Yuksel, J. Akella, S. Kalyanaraman, P. Dutta, Optimal communication coverage for free-space-optical manet building blocks. http://www.shivkumar.org/research/papers/unycn05.pdf, Access date 2014. Also see: CiteSeer × β, Devleoped by Pennsylvania State University, 2007–2010. http://citeseerx.ist.psu.edu/viewdoc/summary?doi=10.1.1.143.5616

28. H. C. van de Hulst, *Light Scattering by Small Particles* (Dover, New York, 1981)